Published in final edited form as:
Osteoarthritis Cartilage. 2008 November ; 16(11): 1395–1402. doi:10.1016/j.joca.2008.03.019.

CHARACTERIZATION OF ARTICULAR CALCIUM-CONTAINING CRYSTALS BY SYNCHROTRON FTIR

Ann K. Rosenthal, MD[**], **Eric Mattson, BS**[*], **Claudia M. Gohr, BS**[**], and **Carol J. Hirschmugl, PhD**[*]

[*] *From the Department of Physics, University of Wisconsin-Milwaukee, Milwaukee, WI*

[**] *the Department of Medicine, Division of Rheumatology, Medical College of Wisconsin, and the Zablocki VA Medical Center, Milwaukee, WI*

Abstract

Objective—Sixty percent of synovial fluids from patients with severe osteoarthritis contain calcium pyrophosphate dihydrate (CPPD) or basic calcium phosphate (BCP) crystals. These bioactive crystals can be particularly difficult to accurately identify in complex biologic systems, such as in vitro models of crystal formation. We sought to determine if synchrotron FTIR (sFTIR) could be used to identify and characterize calcium-containing crystals in mineralization models.

Methods—CPPD and BCP crystals from porcine models of crystal formation were examined with an FTIR Microscope attached to a synchrotron light source. As a comparison, crystals from human synovial fluids were also examined. The sFTIR spectra generated were compared with known spectra of multiple forms of BCP and CPPD crystals, as well as spectra generated by synthetic CPPD and BCP crystals and cartilage proteoglycans, alone and in mixtures.

Results—sFTIR readily identified CPPD and BCP crystals in porcine models as well as in fresh synovial fluids. Brushite was also present in human and porcine samples, and whitlockite was seen in some porcine samples. Mixtures of minerals were commonly found in a single crystal aggregate in both human and porcine samples. In spectra from many CPPD crystals, the peak at the 1134 cm^{-1} found on the standard spectrum for CPPD was diminished. Addition of spectra from cartilage proteoglycans to those of synthetic CPPD crystals dampened the peak at this frequency region, much as this peak was diminished in biologically-derived CPPD crystals.

Conclusion—sFTIR analysis allows for accurate identification of CPPD and BCP crystals generated in vitro and will a useful research tool to study articular crystals.

Keywords

calcium pyrophosphate; calcium phosphate; synchrotron; FTIR; hydroxyapatite; osteoarthritis

INTRODUCTION

Osteoarthritis is the most common form of arthritis in adults and currently affects over 20 million Americans. Calcium-containing crystals, including calcium pyrophosphate dihydrate (CPPD) and hydroxyapatite-like basic calcium phosphate (BCP) crystals are found in 60% of synovial fluids from unselected patients at the time of knee replacement for osteoarthritis (1, 2). BCP crystals are also associated with a severe destructive shoulder arthropathy known as

Corresponding author: Ann K. Rosenthal, MD, Rheumatology Section, cc-111W, Zablocki VA Medical Center, 5000 W. National Ave., Milwaukee, WI 53295-1000, Tel: 414-384-2000, ext 42760, FAX: 414-383-8010, Email: akrose@mcw.edu.

Milwaukee Shoulder Syndrome (3). The presence of CPPD and BCP crystals predict severe radiologic damage and rapid progression of arthritis (2,4).

In the laboratory, CPPD and BCP crystals have catabolic effects on articular tissues. CPPD crystals can induce a vigorous inflammatory response in the joint, inducing the release of catabolic cytokines and proteases from neutrophils and monocytes (5). BCP crystals are also inflammatory under certain conditions (6). Independent of inflammation, both CPPD and BCP crystals have direct catabolic effects on chondrocytes and synovial cells. They induce synovial cell mitogenesis (7), and release collagenase and other matrix-degrading proteases from synoviocytes and chondrocytes (8) (9) (10).

Much about the development of CPPD and BCP crystals in osteoarthritis is poorly understood (11). The current paradigm involves an alteration of the chondrocyte phenotype, induced by aging, injury or osteoarthritis. These chondrocytes assume characteristics similar to those of the hypertrophic chondrocytes that produce bone mineral during epiphyseal growth, such as overproduction of pyrophosphate (PPi), the anionic component of CPPD crystals (12). They also display altered production of key matrix components involved in mineral formation (13). PPi is generated from exogenous ATP by a variety of ectoenzymes, and complexes with ambient calcium to form CPPD crystals (14). Inorganic phosphate can also be generated by chondrocyte ectoenzymes. When phosphate rather than PPi predominates, BCP mineral is generated. Mineral formation occurs in the pericellular matrix, and is facilitated by small chondrocyte-derived extracellular organelles known as articular cartilage vesicles (ACVs) (15).

Progress in understanding the role of calcium-containing crystals in osteoarthritis has been hampered by difficulties in their identification particularly in model systems(16). In clinical samples of joint fluid and cartilage, CPPD crystals can be identified by their characteristic rhomboid morphology and positive birefringence under compensated polarizing light (16). Alizarin red S staining can be used to detect BCP crystals in synovial fluid, but is difficult to interpret and also stains other calcium containing particulates (17). Neither of these techniques is sufficiently sensitive or accurate for research use.

Two well characterized models of calcium crystal formation include a model involving isolated ACVs (15), and a chondrocyte tissue culture model (18). In these models, crystals tend to be very small, relatively sparse, and to be surrounded by debris enriched in proteins, carbohydrates and lipids, which interfere with many identification techniques. Thus, difficulties conclusively identifying the nature and type of calcium crystals produced in these models have limited their use.

Synchrotron FTIR (sFTIR) has been used to study mineralizing tissues, such as bone, as well as cartilage (19) (20). It has proven useful in the study of various factors influencing matrix mineralization in that it can be used quantitatively to estimate amounts and quality of mineral formed (21) (22). Among the many advantages of sFTIR are its high signal to noise ratio, its ability to focus on very small areas in complex specimens, and its usefulness with fresh wet samples, requiring minimal preparation. In addition, the ability to carefully map and characterize substances in the areas in and around individual crystals has great potential for yielding important information about crystal formation and identifying modifiers of this process.

sFTIR can identify calcium-containing crystals generated by in vitro models of crystal formation and illustrates their remarkable similarity to crystals from human synovial fluids. sFTIR will be a useful research tool to further explore the formation and role of calcium-containing crystals in osteoarthritis.

METHODS

Materials

Synthetic CPPD crystals were generated in our laboratory using the method of Brown et al. (23). BCP crystals were a kind gift from Dr. Neil Mandel (National VA Crystal Identification Center, Zablocki VA Medical Center, Milwaukee, WI). Cartilage proteoglycans from human cartilage were purchased from MD Biosciences (St Paul, MN). All other reagents were from Sigma Chemical Co. (St. Louis, MO), unless otherwise specified.

Porcine cartilage

Porcine articular cartilage obtained from the knees of adult pigs (Johnsonville Foods, Inc., Watertown, WI) was used to generate chondrocytes for the tissue culture model and articular cartilage vesicles (ACVs) for the ACV model.

Tissue culture model

A model of CPPD crystal formation in chondrocyte monolayers was described by Ryan et al. (18). In this system, high density primary cultures of normal articular chondrocytes generate CPPD crystals after 3–5 days of incubation with 1 mM ATP. β-glycerophosphate is used as a control for added phosphate. Cartilage pieces were enzymatically treated to remove matrix as previously described and plated at 4×10^5 cells/cm^2 for 2–3 days (24) in Dulbecco's Modified Eagle's Medium (DMEM, Mediatech, Herndon, VA) with 10 % fetal calf serum. Media were replaced with serum-free media for 24 hours, and subsequently exposed to serum-free media containing 1 mM ATP, 1 mM β-glycerophosphate, or no additives for 3–5 days. Media were then removed, and the cell layer was scraped from the plate and subjected to sFTIR analysis.

Articular Cartilage Vesicle (ACV) Model

Cartilage pieces were sequentially exposed to hyaluronidase, trypsin, trypsin inhibitor and collagenase as previously described (15). After an overnight incubation with 0.05% collagenase, the mixture was filtered, centrifuged at 500 g for 15 minutes to remove cells, then at 37,000 g for 15 minutes to remove large cell fragments and organelles. The supernatant was then centrifuged at 120,000 g for 60 minutes to pellet the ACV fraction. Protein concentrations were determined by the Lowry assay (25). The ACV-containing pellet was re-suspended in DMEM to a protein concentration of 12–15 mg/ml and mineralized with calcifying salt solution (15) with or without added ATP or β-glycerophosphate for 3–5 days. After incubation, the crystal-containing pellets were centrifuged, and the supernatants were removed.

Human Synovial Fluids

Samples of human synovial fluids from discarded synovial fluid taken for therapeutic or diagnostic purposes were obtained in accordance with the IRB at the Zablocki VA Medical Center. Five knee fluids containing CPPD crystals as determined by examination under polarizing light microscopy were sealed to prevent drying, refrigerated for further use, and used within 2 weeks of procurement. Two shoulder fluids from patients with clinical Milwaukee Shoulder syndrome in which we expected to find BCP crystals were similarly stored and used. Two knee fluids without CPPD crystals from patients with osteoarthritis were also examined for crystals using sFTIR.

FTIR standards

Standard spectra of basic calcium phosphate (BCP), calcium phosphate (tribasic), and calcium phosphate (monobasic) crystals were obtained from the National Institute for Standards and Technology (NIST) Chemistry Webbook. Standard spectra of triclinic and monoclinic calcium pyrophosphate dihydrate (CPPD) and orthorhombic calcium pyrophosphate trihydrate (O-

CPPT) were obtained from the VA Crystal Identification Library at the Zablocki VA Medical Center.

Spectra of synthetic crystals and cartilage proteoglycans were obtained with a Bruker 66V FT-IR spectrometer. Standard samples of crystals and/or cartilage proteoglycans were compressed into Potassium Bromide (KBr) pellets in a ratio of ~ 19mg KBr: 1mg Sample. The measurements were taken in transmission with 8 cm^{-1} resolution and a 6mm aperture. The infrared spectra were obtained, via mathematical methods available with all commercial infrared spectrometers, from the interferogram, (i.e., the raw data) using a four-point apodization function, which is a mathematical construct to reduce spectral artifacts.

sFTIR

Drop-sized samples from the porcine models or human synovial fluids were applied to Kevley IR reflective slides and examined with plain and compensated polarized light microscopy to locate birefringent or dense materials. These areas were photographed and marked so that the same areas could be examined with sFTIR. The samples were measured with a Thermo Fisher Continuum Fourier Transform-Infrared (FT-IR) microscope coupled to an infrared beamline at the Synchrotron Radiation Center (SRC) in Stoughton, WI. Measurements were taken in reflectance, acquiring reflection-absorbance results. The detector was a mercury-cadmium telluride detector. Both individual spot-measurements and spatially resolved maps of the samples were measured with apertures ranging from 8 μm to 15 μm. The number of scans was selected to optimize the signal-to-noise ratio (SNR). Visible images were collected concurrently. The infrared results were visually compared to reference spectra of multiple forms of calcium-containing crystals and cartilage proteoglycans.

RESULTS

Synovial fluid CPPD and BCP crystals and other crystalline forms are easily identified by sFTIR

Figure 1 displays the absorption standard spectra of BCP and CPPD crystals, as well as visible images from synovial fluid samples. The crosshairs in the visible images indicate the points at which the measurements were obtained. The top sample spectrum was collected with a 10×10μm aperture and 64 scans, while the bottom sample spectrum was collected with an 8×8μm aperture and 64 scans. The infrared signatures produced by the synovial fluid crystals clearly match the standard spectra of monoclinic BCP and CPPD crystals, respectively.

Most CPPD crystals in synovial fluids were monoclinic in morphology. Hydroxyapatite, rather than octacalcium phosphate or tricalcium phosphate accounted for the majority of the BCP crystals in synovial fluid. Brushite ($Ca(HP0_4)\cdot 2H_20$) was also identified in several synovial fluids (Figure 2). It occurred alone and in combination with CPPD. As illustrated in figure 1, amine peaks at 1598–1710 cm^{-1}, and 1492–1598 cm^{-1} were commonly seen in association with crystals, supporting the presence of protein in or around crystals. The carbohydrate peak characteristic of proteoglycans is typically seen at 950–1150 cm^{-1} (26), and overlaps one of the signature CPPD peaks.

Both CPPD and BCP crystals are present in mineralized ACV samples

Two images of spectra from crystals formed by ACVs are shown in Figure 3, along with the standard infrared spectra for BCP and CPPD crystals. The crosshair identifies the point at which the image was collected for each sample. The data for the CPPD standard and ACV-generated crystal have been multiplied by two and offset below 1500 cm^{-1} to emphasize the comparison between the spectra. One can see that the spectrum for the top sample is similar to BCP and that the spectrum for the bottom sample is similar to monoclinic CPPD. Thus, not surprisingly,

ACVs are capable of generating both types of crystals. While both forms of crystals were seen in many samples regardless of the phosphate source, CPPD predominated in samples incubated with ATP, and BCP crystals in samples incubated with β-glycerophosphate. Brushite and whitlockite were also noted in these samples. (Data not shown). As in synovial fluids, crystal-containing spectra in the ACV preparations tended to include amine (protein) peaks.

CPPD crystals identical to those found in synovial fluid are present in chondrocyte monolayers incubated with ATP

Figure 4 shows a comparison of spectra for CPPD crystals produced in porcine chondrocyte monolayers and CPPD crystals in human synovial fluid. The bottom spectrum was collected from chondrocyte monolayers incubated with ATP. The top spectrum was collected from a sample of human synovial fluid. Note that the infrared absorbance is very similar for the samples from the two models. However one of characteristic features of the CPPD spectrum, the asymmetric stretch of the POP functional group represented by the peak seen at 916–972 cm^{-1}, is slightly weaker on the crystal created from the chondrocyte monolayers that those from ACVs or synovial fluids. Whether this is related to the orientation of the crystal at the time at which it was measured is not clear, but this possibility is currently being investigated.

Unlike ACVs, chondrocyte monolayers do not appear to generate pure BCP crystals. Although an exhaustive search for BCP crystals was not undertaken, BCP mineral only appeared in conjunction with CPPD mineral.

Crystals in porcine models and synovial fluids contain many regions that are mixtures of mineral as well as proteoglycans

We also noted that many individual crystals contained regions that did not exactly match either pure CPPD or pure BCP crystals, and investigated the possibility that these regions contained both CPPD and BCP mineral. Figure 5 shows a typical spectrum from a crystal generated by chondrocyte monolayers treated with ATP. It was almost an identical match to a combination of 30% CPPD and 20% BCP (Data not shown). However, we frequently noted that the peak at 1134 cm^{-1} of CPPD in both human and porcine samples was often blunted compared to the spectra generated by synthetic monoclinic CPPD crystals, and wondered about the contribution of carbohydrate moieties to this blunting. The carbohydrate peak is located at 950–1150 cm^{-1} and might logically alter the CPPD peak at 1134 cm^{-1}. Figure 5 shows a spectrum from this crystal compared with a standard spectrum generated from a combination of 50% proteoglycans, 30% monoclinic CPPD, and 20% BCP. The addition of the proteoglycan spectrum resulted in blunting of the CPPD peak at 1134 cm^{-1} similar to that seen in the biologic samples. These findings support the presence of proteoglycans on or near CPPD crystals and explain the altered morphology of this signature peak in many biologic samples.

This technology allows for careful mapping of an individual crystal

BCP and CPPD crystals, as well as mixtures of the two, were found within close proximity to each other. Figure 6 is a map from a crystal generated by ACVs, while figure 7 is a map from a synovial fluid crystal. Oversampling was used, collecting infrared spectra in 8 micron steps to achieve higher quality resolution on the maps. A total of 110 (10×11) pixels are displayed on the maps.

The ACV-generated crystal was mapped in regards to CPPD and BCP. Panel B represents the visible image, while panels A and C are infrared images of the visible image. Red areas on the infrared images indicate areas with high absorption and are indicative of marked similarity to the functional group, whereas blue areas indicate low amounts of absorption by the functional group in question, and are areas that are very different from the functional group. Panel A is an infrared image where red color indicates similarity to BCP mineral and is integrated over

950–895 cm^{-1}. Similarly, panel C is an infrared map where red indicates strong similarity to CPPD mineral and is integrated over 1015–1150 cm^{-1}. Points 1 to 5 indicate specific spectra at these points on the map, and most match best with a mixture of CPPD, BCP and brushite.

For the synovial fluid crystal (Figure 7), profiles indicating the absorbance of a particular functional group were calculated on the map for different functional groups specific to BCP and CPPD, respectively. The functional group used to identify BCP occupied the region from 985–1155 cm^{-1}, and this is shown in panel A, while the functional group specific to CPPD occupied the region from 1125–1201 cm^{-1} is shown in panel C. Panel B represents the visible image. The map suggests superimposed or adjacent areas of CPPD and BCP mineral in a single crystal aggregate.

DISCUSSION

We show here that sFTIR can be used to conclusively identify CPPD and BCP crystals in low frequency, high background samples such as biologic models. Clearly, while this technology will remain a research tool, it has important implications for our understanding of these crystals in disease. sFTIR has many advantages over traditional methods of crystal identification. In contrast to x-ray diffraction and traditional FTIR, it requires minimal sample preparation, limiting concerns about creating artifactual crystals or further reducing already sparse crystals. It can be performed with a single drop of crystal-containing sample, and its high signal to noise ratio and is ideally suited to characterize these tiny crystals in a sea of other components. Furthermore, the polarized quality of the synchrotron beam may yield important information about crystal polarity that may reveal clues as to how these pathogenic crystals grow.

This technology is not without limitations, however. Measurements of samples containing large quantities of relatively pure crystal can be easily performed in a laboratory with a similar infrared microscope. Measurements of less pure samples with small and sparse crystals require access to a synchrotron source. There are only four national synchrotron user facilities equipped with the proper facilities to perform these experiments; so access to this technology is certainly limited and requires considerable expertise and potential expense.

These studies reinforce the validity of these *in vitro* models of crystal formation and provide important information about these models. While conventional FTIR studies demonstrated the presence of CPPD and BCP crystals in ACVs, until now, CPPD crystals in the monolayer model had only been putatively identified (18). The absence of pure BCP crystals in the monolayer model also has important implications about the process of crystal formation. This corroborates previous studies showing that adding phosphate to chondrocyte monolayers produces no increase in calcification, while adding ATP strongly stimulates mineralization (13). In contrast, ACVs mineralize with the addition of phosphate or ATP. While monolayers and ACVs share similar mineralization regulating enzymes, it is likely that the extracellular matrix surrounding chondrocytes in monolayer culture permits CPPD crystal formation in the presence of ATP, but prevents BCP mineral from forming.

We were quite surprised at the numbers of crystal aggregates that contained both CPPD and BCP mineral. Although CPPD and BCP crystals commonly co-exist clinically (27), their relationship to one another etiologically and in cartilage remains controversial. For example, in intact human cartilage, Pritzker et al. found only 2 of 23 samples of cartilage with CPPD crystal deposits also contained BCP crystals (28). They based their findings on morphologic differences between the crystal types as well as electron diffraction results obtainable only with sufficient hydroxyapatite loads. Synovial fluid studies, however, suggest a much more common coexistence, and Gordon et al. noted frequent calcifications in cartilage affected by OA, but were unable to further characterize these deposits (29). While a paucity of pure BCP crystals

was certainly reflected in our monolayer model, many CPPD crystals from both human and porcine samples contained some BCP mineral. PPi can inhibit BCP crystal growth (30), but whether BCP crystals can coat the surface and limit the size of CPPD crystals remains unclear.

Crystals were always found in association with protein, and in the case of CPPD crystals, proteoglycans were often present. The interference of the carbohydrate peak with one of the characteristic spectral peaks of CPPD, explains why the peaks of biologic crystals may not exactly match reference FTIR spectra. It also suggests that proteoglycans, which are traditionally considered inhibitors of mineralization, are found in close contact with crystals. It is difficult to discern from our data whether crystals are coated with protein or proteoglycan or these substances are mixed within the crystal itself. Further work to determine the spatial relationships of crystal components by measuring spectra in transmission rather than reflectance, is ongoing in our laboratory and may yield this important information.

Previous studies have used FTIR with or without a synchrotron light source to investigate cartilage in osteoarthritis. For example, Bi et al. recently used a similar technique without a synchrotron-generated beam to non-invasively characterize changes in articular cartilage in a model of rabbit OA (26). They correlated collagen and proteoglycan content with the area under certain peaks and could also examine collagen degradation using a peak at 1338 cm^{-1}. Other studies have used sFTIR to measure mineral quantity in bone as well as to determine the matrix to mineral ratio, a key measure of bone “quality”. It is hoped that the application of this technique to crystals in situ in articular cartilage may yield similar quantitative information as well as important information about changes in the extracellular matrix that may regulate mineral formation.

We were also able to document the presence of brushite in both human and porcine samples. Brushite is a hydrated form of calcium phosphate that has an inflammatory potential similar to that of hydroxyapatite (31). It has also been proposed to be one of the earliest forms of calcium phosphate crystal generated during bone mineralization (32) and may appear similar radiographically to chondrocalcinosis (33). The role of brushite in arthritis and the conditions favoring its formation certainly warrant further investigation.

Whitlockite was seen in the porcine samples but not in synovial fluid samples, and the significance of this finding is uncertain. Whitlockite and other magnesium-containing calcium phosphate crystals are well documented in normal and osteoarthritic articular cartilage (34), and recently have been seen in human intervertebral discs alone and in association with CPPD crystals (35). They are less inflammatory then non-magnesium containing calcium crystals (36). These interesting crystals are also found in cases of metastatic pulmonary calcification complicating end stage renal disease (37), as well as in other forms of pathologic calcification (38).

In summary, we show here that sFTIR can be used to identify small and sparse calcium-containing crystals in models of crystal formation as well as in human synovial fluids. Brushite and whitlockite were identified in these samples. These findings reinforce the frequent occurrence of both CPPD and BCP crystals in a single crystal aggregate. They emphasize the common association of crystals with proteins and proteoglycan and validate the monolayer model of CPPD crystal formation. Further application of this exciting technology should give us additional information about these important crystals.

Acknowledgements

This work was supported by NIH grant AR-RO1-052615 (AKR). We greatly appreciate the assistance of Dr. Neil Mandel and Kathleen Fryjoff with the National VA Crystal Identification Center, Dr. Lawrence Ryan for his generous

gift of time and sage scientific advice, and the Synchrotron Radiation Center, which is funded by National Science Foundation Award No. DMR-0537588 and the University of Wisconsin-Madison.

References

1. Derfus B, Kurian J, Butler J, Daft L, Carrera G, Ryan L, et al. The high prevalence of pathologic calcium crystals in pre-operative knees. J Rheumatol 2002;29:570–4. [PubMed: 11908575]
2. Nalbant S, Martinez J, Kitumnuaypong T, Clayburne G, Sieck M, Schumacher H Jr. Synovial fluid features and their relations to osteoarthritis severity: new findings from sequential studies. Osteoarthritis Cart 2003;11:50–4.
3. Halverson P, Cheung H, McCarty D, Garancis J, Mandel N. Milwaukee Shoulder: Association of microspheroids containing hydroxyapatite crystals, active collagenase and neutral protease with rotator cuff defects: II. Synovial fluid studies. Arthritis Rheum 1981;24:474–54. [PubMed: 6260121]
4. Bardin T, Bucki B, Lansaman J, Lequesne M, Dryll A, Kuntz D. Calcium crystals and rapidly destructive osteoarthritis (Abstract). Osteoarthritis and Cartilage 1993;1:15.
5. Landis R, Haskard D. Pathogenesis of crystal-induced inflammation. Curr Rheum Reports 2001;3:36–41.
6. Prudhommeaux F, Schlitz C, Liote F, Ali H, Champy R, Bucki B, et al. Variation in the inflammatory properties of basic calcium phosphate crystals according to crystal type. Arthritis Rheum 1996;39:1319–26. [PubMed: 8702440]
7. McCarthy G, Mitchell P, Cheung H. The mitogenic response to basic calcium phosphate crystals is accompanied by collagenase induction and secretion in human fibroblasts. Arthritis Rheum 1991;34:1021–8. [PubMed: 1650221]
8. McCarthy G, Mitchell P, Struve J, Cheung H. Basic calcium phosphate crystals cause coordinate induction and secretion of collagenase and stromelysin. J Cell Physiol 1992;153:140–6. [PubMed: 1325976]
9. McCarthy G, Westfall P, Masuda I, Christopherson P, Cheung H, Mitchell P. Basic calcium phosphate crystals activate human osteoarthritic synovial fibroblasts and induce matrix metalloproteinase-13 (collagenase-3) in adult porcine articular chondrocytes. Ann Rheum Dis 2001;60:399–406. [PubMed: 11247873]
10. Ea H-K, Uzan B, Rey C, Liote F. Octacalcium phosphate crystals directly stimulate expression of inducible nitric oxide synthase throgh p38 and JNK mitogen-activated protein kinases in articular chondrocytes. Arthritis Res 2005;7:R915–26.
11. Rosenthal A. Update in calcium deposition diseases. Curr Opin Rheumatol 2007;19:158–62. [PubMed: 17278931]
12. Ryan L, Kurup I, Rosenthal A, McCarty D. Stimulation of pyrophosphate elaboration by cultured cartilage and chondrocytes. Arch Biochem Biophys 1989;272:393–9. [PubMed: 2546499]
13. Rosenthal A, Gohr C, Uzuki M, Masuda I. Osteopontin promotes pathologic mineralization in articular cartilage. Matrix Biol 2007;26:96–105. [PubMed: 17123806]
14. Costello J, Ryan L. Modulation of chondrocyte production of extracellular inorganic pyrophosphate. Curr Opin Rheum 2004;16:268–72.
15. Derfus B, Rachow J, Mandel N, Boskey A, Buday M, Kushnaryov V, et al. Articular cartilage vesicles generate calcium pyrophosphate dihydrate-like crystals in vitro. Arthritis Rheum 1992;35:231–240. [PubMed: 1734912]
16. Rosenthal A, Mandel N. Identification of crystals in synovial fluids and joint tissues. Current Rheumatology Reports 2001;3:11–6. [PubMed: 11177766]
17. Gordon C, Swan A, Dieppe P. Detection of crystals in synovial fluid by light microscopy: sensitivity and reliability. Annals of Rheumatic Diseases 1989;48:737–742.
18. Ryan L, Kurup I, Derfus B, Kushnaryov V. ATP-induced chondrocalcinosis. Arthritis Rheum 1992;35:1520–4. [PubMed: 1472129]
19. Marcott C, Reeder R, Paschalis E, Tatakis D, Boskey A, Mendelsohn R. Infrared microscpectroscopic imaging of biomineralized tissues using a mercury-cadmium-telluride focal-plane array detector. Cell Mol Biol 1998;44:109–15. [PubMed: 9551643]

20. Sato M, M W, Miyoshi N, Imamura Y, Noriki S, Uchida K, et al. Hydroxyapatite maturity in the calcified cartilage and underlying subchondral bone of guinea pigs with spontaneous osteoarthritis: Analysis by Fourier Transform Infrared Microspectroscopy. Acta Histochem Cytochem 2004;37:101–7.
21. Paschalis E, Jacenko O, Olsen B, Decrombrugghe B, Boskey A. The role of type X collagen in endochondral ossification as deduced by Fourier Transform Infrared Microscopy Analysis. Conn Tissue Res 1996;35:371–7.
22. Miller L, Vairavamurthy V, Chance M, Mendelsohn R, Pachalis E, Betts F, et al. In situ analysis of mineral content and crystallinity in bone using infrared micro-spectroscopy of the v4 PO43- vibration. Biochim Biophys Acta 2001;1527:11–19. [PubMed: 11420138]
23. Brown E, Lehr J, Smith A. Preparation and characterization of some calcium pyrophosphates. Agric Food Chem 1963;11:214–22.
24. Rosenthal A, Cheung H, Ryan L. Transforming growth factor beta 1 stimulates inorganic pyrophosphate elaboration by porcine cartilage. Arthritis Rheum 1991;34:904–911. [PubMed: 1647773]
25. Lowry O, Rosebrough N, Farr A, Randall R. Protein measurement with Folin-phenol reagent. J Biol Chem 1951;193:265–75. [PubMed: 14907713]
26. Bi X, Yan X, Bostrom M, Bartusik D, Ramaswamy S, Fishbein K, et al. Fourier transform infrared imaging and MR microscopy studies detect compositional and structural changes in cartilage in rabbit model of osteoarthritis. Anal Bioanal Chem 2007;387:1601–12. [PubMed: 17143596]
27. Hamilton E, Pattrick M, Hornby J, Derrick G, Doherty M. Synovial fluid calcium pyrophosphate dihydrate crystals and alizarin red positivity: analysis of 3000 samples. Br J Rheumatol 1990;29:101–4. [PubMed: 2157516]
28. Pritzker K, Cheng P-T, Renlund R. Calcium pyrophosphate crystal deposition in hyaline cartilage: Ultrastructural analysis and implications for pathogenesis. J Rheumatolo 1988;15:828–35.
29. Gordon G, Villanueva T, Schumacher H, Gohel V. Autopsy study correlating degree of osteoarthritis, synovitis and evidence of articular calcification. J Rheumatol 1984;11:681–6. [PubMed: 6096542]
30. Hearn, P.; Guilland-Cumming, P.; Russell, R. Ann Rheum Dis. 42. 1983. Effect of orthophosphate and other factors on the crystal growth of calcium pyrophosphate in vivo; p. 101
31. Higson F, Jones O. Oxygen radical production by horse and pig neutrophils induced by a range of crystals. J Rheumatol 1984;11:735–40. [PubMed: 6097690]
32. Howell D, Pita J, Marquez J, Madruga J. Partition of calcium, phosphate, and protein in the fluid phase aspirated at calcifying sites in epiphyseal cartilage. J Clin Invest 1968;47:1121–32. [PubMed: 5645857]
33. Rosenthal, A.; Ryan, L. Calcium Pyrophosphate Crystal Deposition Diseases, Pseudogout, and Articular Chondrocalcinosis. In: Moreland, WJK., editor. Arthritis and Allied Conditions. Philadelphia: Lippincott Williams & Wilkins; 2004. p. 2373-96.
34. Ali S. Apatite-type crystal deposition in arthritic cartilage. Scanning Electron Microscopy 1985;4:1555–66. [PubMed: 4095501]
35. Lee R, Kayser M, Ali S. Calcium phosphate microcrystal deposition in the human intervetrebral disc. J Anat 2006;208:13–9. [PubMed: 16420375]
36. Ryan L, Cheung H, LeGeros R, Kurup I, Toth J, Westfall P, et al. Cellular responses to whitlockite. Calcif Tissue Int 1999;65:374–7. [PubMed: 10541763]
37. Eggert C, Albright R. Metastatic pulmonary calcification in a dialysis patient: case report and a review. Hemodialysis Int 2006;10:S51–5.
38. Lagier R, Baud C. Magnesium whitlockite, a calcium phosphate crystal of special interest in pathology. Pathol, Res & Prac 2003;199:329–35.

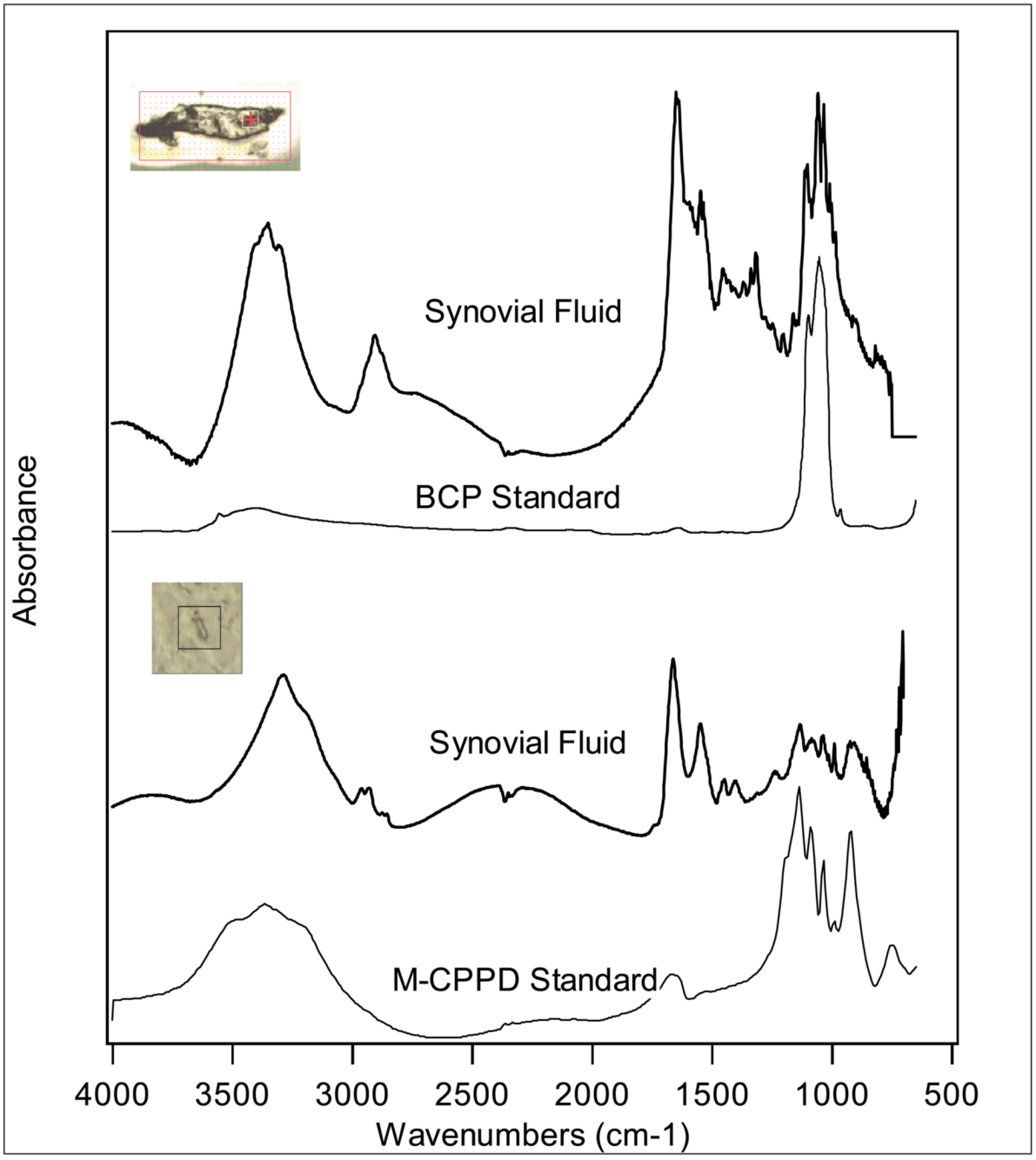

Figure 1. Representative sFTIR spectra from human synovial fluids demonstrating CPPD and BCP crystals

The crosshairs in the visible images indicate the points at which the measurements were obtained. The top sample spectrum was collected with a 10×10μm aperture and 64 scans, while the bottom sample spectrum was collected with an 8×8μm aperture and 64 scans. For the latter crystal, the sample is clearly smaller than the 8×8 aperture, but is completely within the field of view. The infrared signatures produced by the synovial fluid crystals clearly match the standard spectra of BCP and CPPD crystals, respectively. The additional peaks on the synovial fluid crystal spectra suggest the presence of biologic material mixed with the crystals.

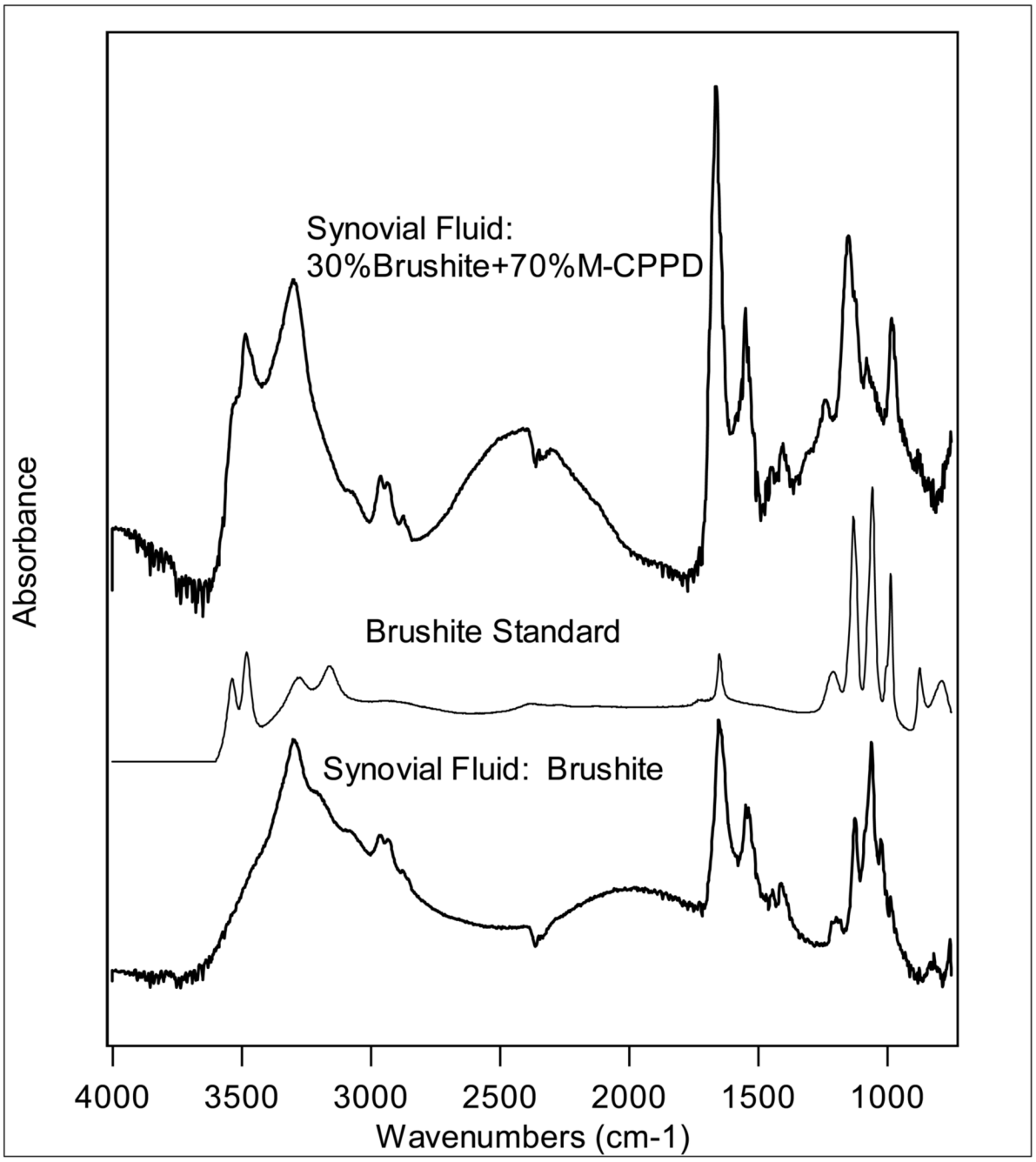

Figure 2. Representative sFTIR spectra from human synovial fluid demonstrating brushite alone and in combination with CPPD crystals

Two crystals from human synovial fluids were characterized and compared to a brushite standard. The top spectrum represents a crystal containing both CPPD and brushite components, while the bottom spectrum appears to be pure brushite. The bottom spectrum was measured with an 8×8 micron aperture, and the top one was measured with a 10×10 micron aperture. Both measurements were collected with 64 scans.

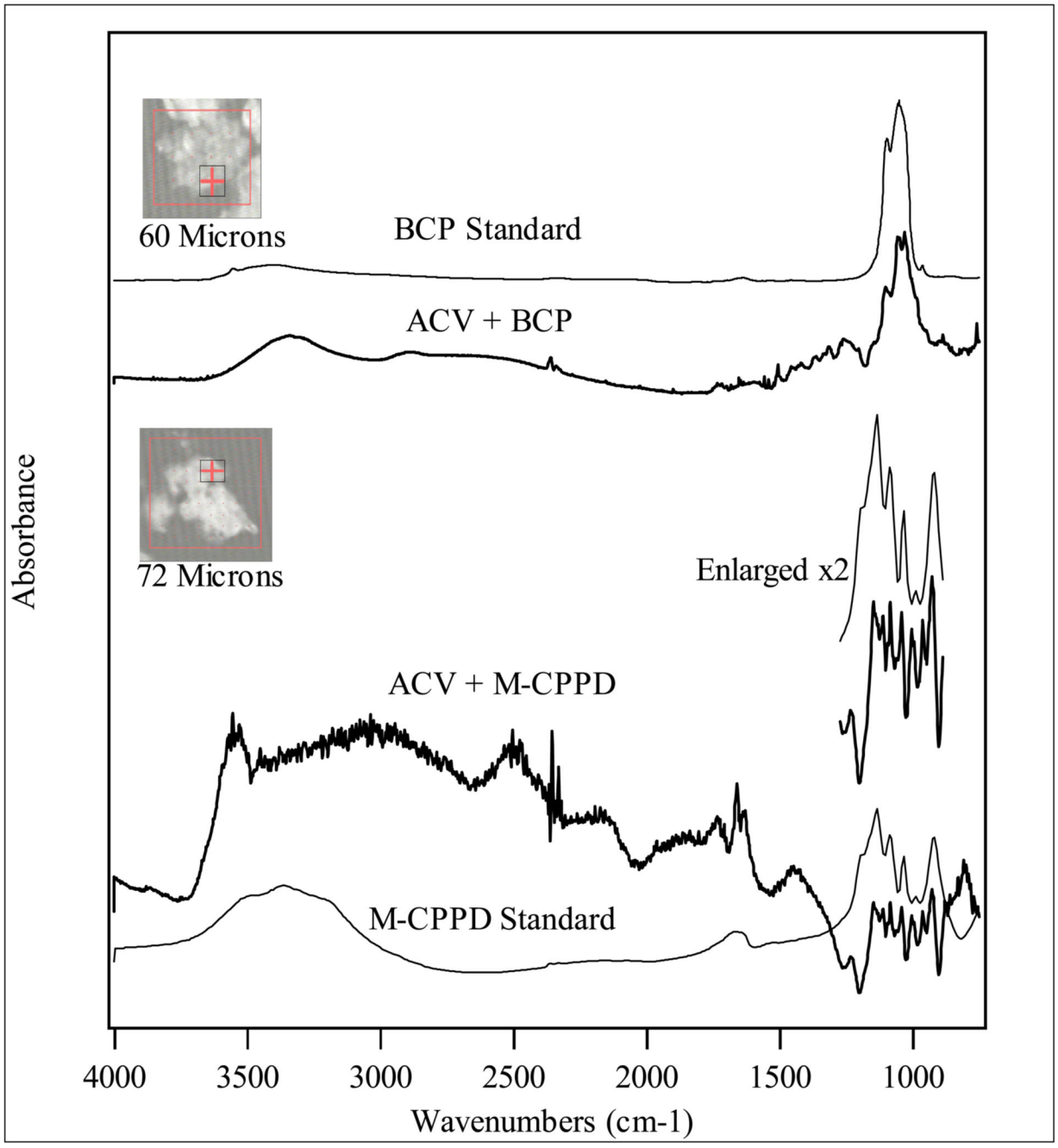

Figure 3. Representative sFTIR spectra from porcine ACVs

ACVs were incubated for 3–5 days with either 1 mM ATP or 1 mM β glycerophosphate.. The crosshair identifies the point at which the image was collected for each sample. The top sample spectrum was collected a 15×15μm aperture as shown and 64 scans, while the bottom sample spectrum was collected with a 12×12μm aperture as shown and 64 scans. The data for the monoclinic CPPD (mCPPD) standard and the ACV-generated CPPD-like crystal have been multiplied by two and offset below 1500 cm^{-1} to emphasize the comparison between the spectra. The spectrum for the top sample is similar to BCP and that the spectrum for the bottom sample is similar to monoclinic CPPD.

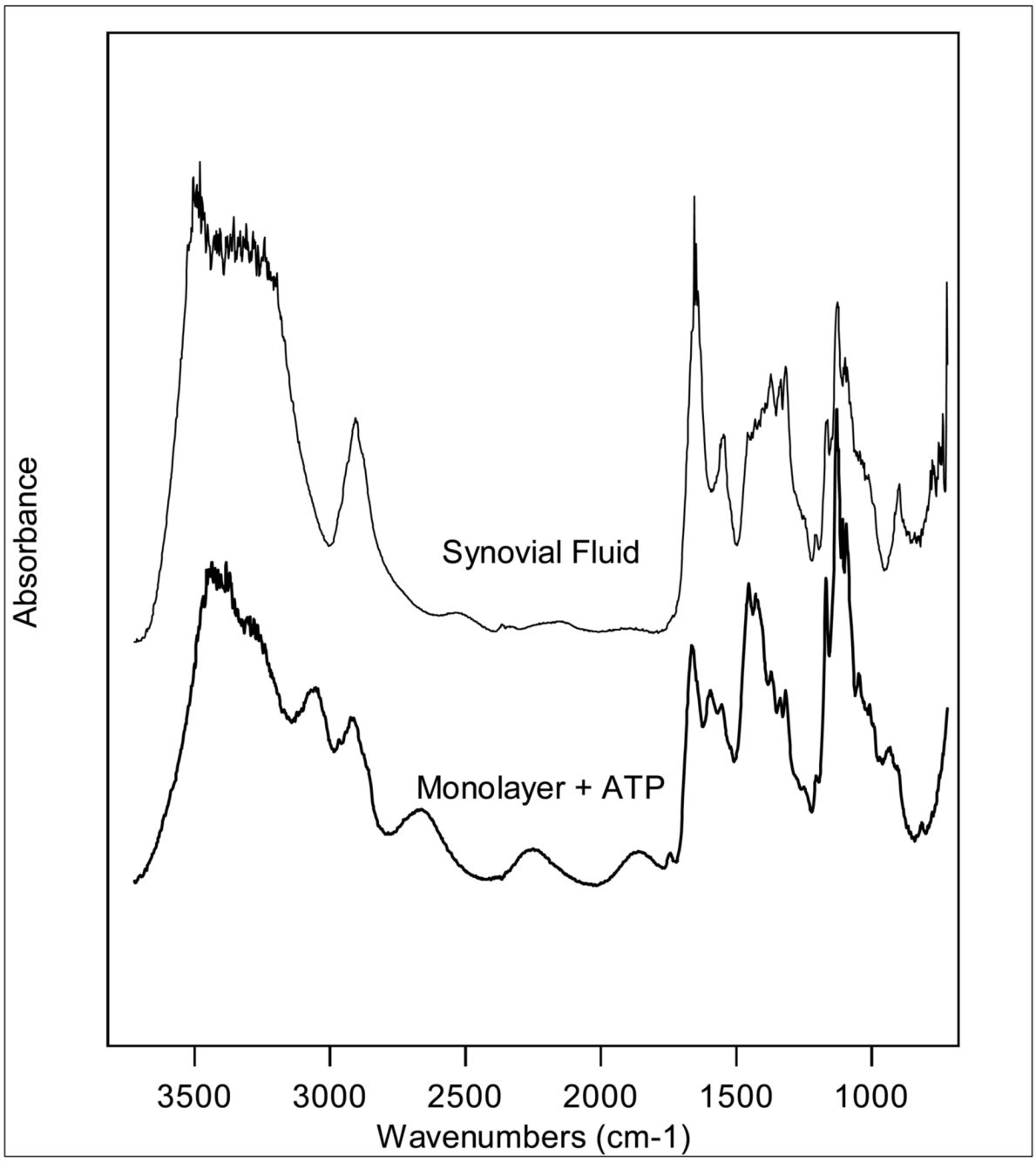

Figure 4. Representative sFTIR spectra from porcine chondrocyte monolayers compared to human synovial fluid

Chondrocyte monolayers were incubated with ATP for 72 hours. A crystal from these monolayers was compared with a CPPD crystal from human synovial fluid. The chondrocyte spectrum was collected with a 12×12μm aperture and 64 scans. The synovial fluid spectrum was collected with a 10×10μm aperture and 64 scans. These spectra are virtually identical.

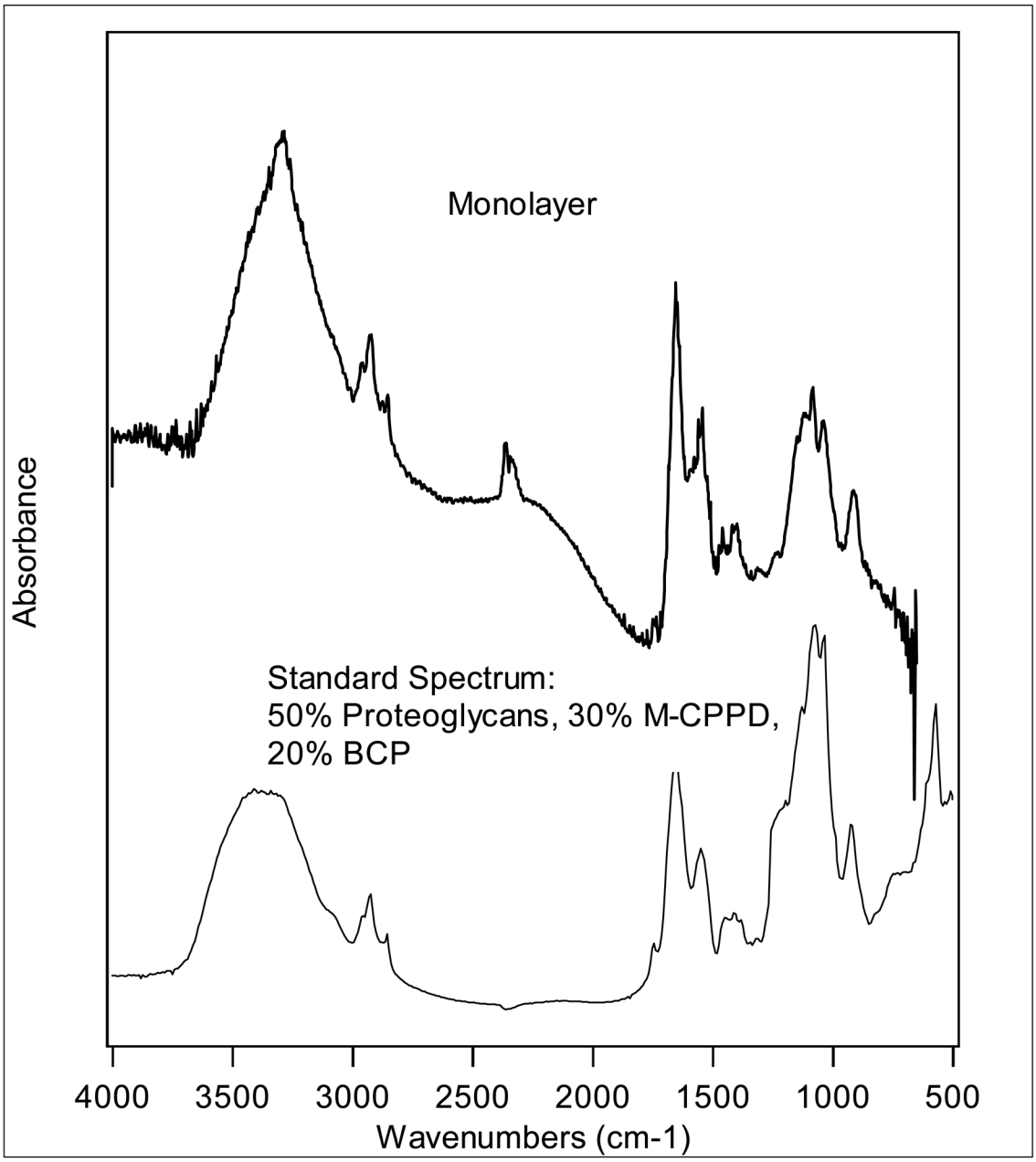

Figure 5. Representative sFTIR spectrum from a crystal generated by chondrocyte monolayers and a mixture of BCP, CPPD and proteoglycans

The sFTIR spectrum from a crystal generated by chondrocyte monolayers was compared with an FTIR spectrum generated by a combination of 50% cartilage proteoglycans, 30% monoclinic CPPD, and 20% BCP.

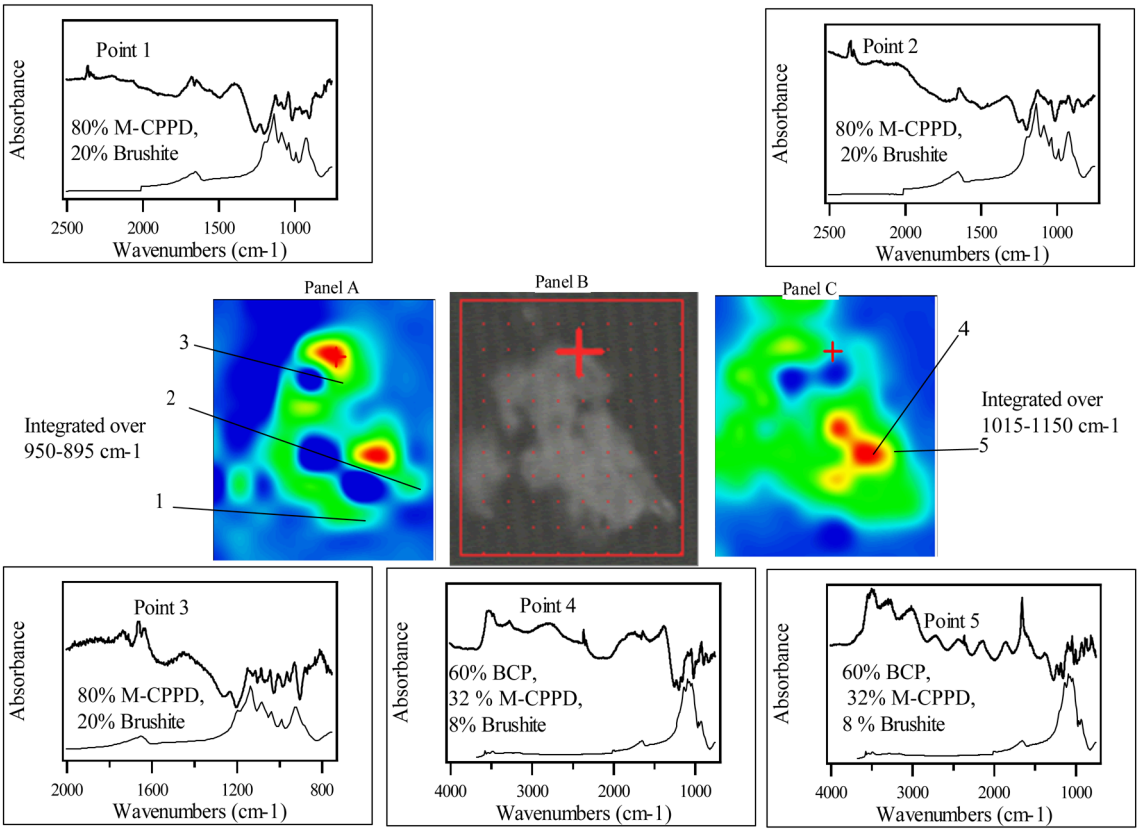

Figure 6. sFTIR map of a typical crystal generated by ACVs

The data, 110 pixel over the entire area were collected with 12 ×12 μm aperture and 64 scans per pixel. Panel B shows a visible image of the crystal with red dots showing the location of each pixel of data. Infrared images (Panels A and C) are shown that are dominated by the absorbance of functional groups specific to BCP (Panel A) and CPPD (panel C). The spectral range for BCP was 985–895 cm $^{-1}$ and for CPPD was 1015–1150 cm $^{-1}$. Red areas on the infrared images indicate high absorption intensity and can be indicative of the presence of the crystal functional group, whereas blue areas indicate low absorption intensity by functional group and absence of the functional group. The remaining panels (points 1–5) show standard spectra and data in a given pixel for the pixels identified in the infrared images and compare them to combinations of CPPD, BCP and brushite. All of the sample spectra contain additional peaks arising from admixture of biologic material. The infrared images and spectra suggest superimposed areas of CPPD, BCP and brushite mineral in a single crystal aggregate.

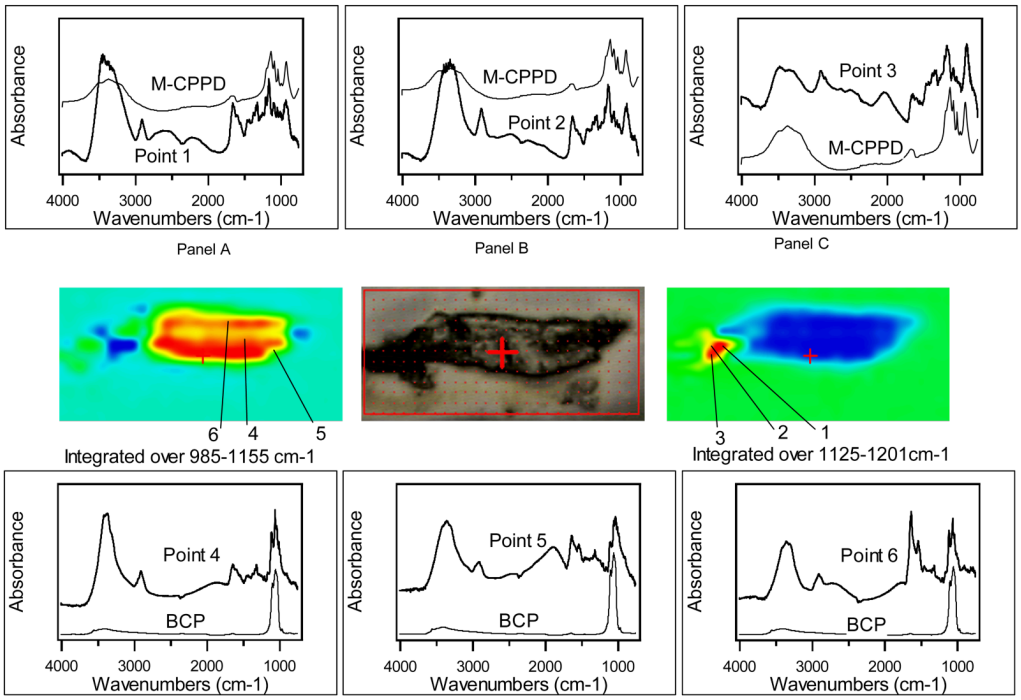

Figure 7. sFTIR map of a synovial fluid crystal

The data, 110 pixels over the entire area were collected with a 12×12μm aperture and 64 scans per pixel. Panel B shows a visible image of the crystal, while infrared images in panels C and E are dominated by the absorbance of functional groups suggestive of CPPD (1125–1201 cm^{-1}) or BCP (985–1155 cm^{-1}). Red areas on the infrared images indicate high absorption intensity and are indicative of the presence of the crystal functional group, while blue areas indicate low absorption and relative scarcity of the functional group. The remaining panels (points 1–6) show standard spectra and data in a given pixel for the pixels identified in the infrared images. The infrared images and spectra suggest adjacent areas of CPPD and BCP in a single crystal aggregate.